

Article

Siderite Formation by Mechanochemical and High Pressure–High Temperature Processes for CO₂ Capture Using Iron Ore as the Initial Sorbent

Eduin Yesid Mora Mendoza ^{1,2,*}, Armando Sarmiento Santos ¹, Enrique Vera López ¹, Vadym Drozd ², Andriy Durygin ² , Jiuhua Chen ² and Surendra K. Saxena ²

¹ Grupo de Superficies, Electroquímica y Corrosión, GSEC, Instituto para la Investigación e Innovación en Ciencia y Tecnología de Materiales, INCITEMA, Universidad Pedagógica y Tecnológica de Colombia UPTC, Tunja 150008, Colombia; asarmiento.santos@uptc.edu.co (A.S.S.); enrique.vera@uptc.edu.co (E.V.L.)

² Center for the Study of Matter at Extreme Conditions, Department of Mechanical and Materials Engineering, College of Engineering and Computing, Florida International University, Miami, FL 33199, USA; drozdv@fiu.edu (V.D.); durygina@fiu.edu (A.D.); chenj@fiu.edu (J.C.); saxenas@fiu.edu (S.K.S.)

* Correspondence: eduin.mora@uptc.edu.co

Received: 6 September 2019; Accepted: 5 October 2019; Published: 14 October 2019



Abstract: Iron ore was studied as a CO₂ absorbent. Carbonation was carried out by mechanochemical and high temperature–high pressure (HTHP) reactions. Kinetics of the carbonation reactions was studied for the two methods. In the mechanochemical process, it was analyzed as a function of the CO₂ pressure and the rotation speed of the planetary ball mill, while in the HTHP process, the kinetics was studied as a function of pressure and temperature. The highest CO₂ capture capacities achieved were 3.7341 mmol of CO₂/g of sorbent in ball milling (30 bar of CO₂ pressure, 400 rpm, 20 h) and 5.4392 mmol of CO₂/g of absorbent in HTHP (50 bar of CO₂ pressure, 100 °C and 4 h). To overcome the kinetics limitations, water was introduced to all carbonation experiments. The calcination reactions were studied in Argon atmosphere using thermogravimetric analysis (TGA) and differential scanning calorimetry (DSC) analysis. Siderite can be decomposed at the same temperature range (100 °C to 420 °C) for the samples produced by both methods. This range reaches higher temperatures compared with pure iron oxides due to decomposition temperature increase with decreasing purity. Calcination reactions yield magnetite and carbon. A comparison of recyclability (use of the same material in several cycles of carbonation–calcination), kinetics, spent energy, and the amounts of initial material needed to capture 1 ton of CO₂, revealed the advantages of the mechanochemical process compared with HTHP.

Keywords: CO₂ capture; iron ore; carbonation; calcination; recyclability; mechanochemical reactions; carbonation kinetics

1. Introduction

The planet temperature has been monitored since the 19th century, however only since the 1980s has the world realized that global warming was occurring, according to Goddard Institute for Space Studies (GISS) report [1]. The global temperature has increased in the last 50 years by about 1 °C. CO₂ atmospheric concentration rose to 401 ppm in 2015, which is an increase of 110 ppm since the start of the industrial age [1–3]. Even though some countries have defined policies using international deals, such as Rio de Janeiro (1992), Kyoto (1997), and Copenhagen (2009), the global warming problem remains. A premise in the Paris agreement (2016) is to invest more than 100 billion dollars a year to achieve a solution to the green-house effect of gasses emission. Indeed, these agreements have helped

to develop and improve different strategies and technologies to reduce the amount of CO₂ emitted to the atmosphere, as it is the main cause of the green-house effect [3–5].

Renewable energy and energy-efficient use as preventive approaches to reduce CO₂ emissions are still far from suitable solutions. Several techniques can be used for CO₂ separation from flue gases and its subsequent sequestration. These are classified as either physical and chemical methods. The chemical absorption reactions use chemical absorbents, such as amines, and are the most mature technology. Although absorption by amine is the method mainly used in industry, the required energy for the absorbents' regeneration is considerably high [6–8]. Membranes are not considered as applicable solutions due to low mass transfer [9,10]. However, some recent studies have shown remarkable improvements in the CO₂/N₂ selectivity of the membranes [10]. Cryogenics and microalgals are laboratory-scale technologies [11].

As a result of an exothermic reaction, carbonates generated from metallic oxides, such as MgO, FeO, or CaO, and carbon dioxide, which can be taken from flue gases, are a suitable means of capturing CO₂. These carbonates can be heated, and after that, using an endothermic reaction, pure CO₂ is released. This pure gas can be used in valuable industrial applications, such as oil recovery oil in the food industry, etc., allowing the recovery of the metal oxides, which, in turn, can be used in a new cycle of carbonation–calcination until the active sites disappear [5,12]. Iron oxides have good thermodynamic properties to be a CO₂ sorbent. Kumar et al. [13] demonstrated that a mixture of magnetite and iron can be carbonated with 57% conversion efficiency by adding water as a catalyst. Graphite and iron are suitable reducing agents for carbonation. In addition, they are highly available in steel making industries. Recent research found a novel way to carbonate iron oxides and iron using a ball milling process, reaching almost pure siderite without the use of water [14].

In addition, wustite, hematite, magnetite, and even siderite, iron ore can contain different compounds, such as CaO, MnO, Al₂O₃, K₂O, S, SiO₂, P₂O₅ [15]. Siderite is used in industrial processes. Hence, its thermal decomposition has generated interest. Depending on the atmosphere, different calcination products are formed. Hematite (Fe₂O₃) is common in an oxidizing atmosphere. Magnetite is obtained in a CO₂ atmosphere, while magnetite and wustite (FeO) are found in an inert atmosphere or in vacuum [14,16,17].

In this work, the CO₂ capture capacity of iron ore from the El Uvo mine, Colombia, was studied. Thermodynamic simulations supported the results of carbonation–calcination reactions. The CO₂ capture capacity was studied for the HTHP process as a function of pressure, temperature, and reaction time, while in the ball milling process, it was studied as a function of pressure, revolution speed, and reaction time. The kinetics of mechanochemical reactions was studied, and finally, energy spend in both carbonation methods was compared.

2. Experimental

The iron ore samples were prepared from a mineral rock, which was crushed and ground using a mortar and pestle, and, finally, processed by ball milling in an inert atmosphere for two hours. The chemical composition of the ore was studied by X-ray fluorescence analysis (XRF), as shown in Table 1. The major component was iron, but there are some impurities, such as SiO₂, CaO, Al₂O₃, MgO, MnO, P₂O₅, Na₂O, K₂O, S, and Zn.

The reactor for carbonation in the HTHP process was a closed cylindrical vessel of length 31.75 mm and an internal diameter of 8.89 mm. The reactor was loaded with 0.25 g of iron ore and iron (Good Fellow, 99% purity, <60 μm) mixture. The molar ratio of iron ore/Fe was defined according to the stoichiometry of reactions (1) and (2).



Zero-point one five milliliters of water was added to the vessel to improve the kinetics of the carbonation reaction. High purity CO₂ gas (99.99% purity, Airgas) was introduced into the system at desired pressures from 30 to 50 bar. Before the experiments, the reactor was flushed with CO₂ gas three times to ensure an inert atmosphere in the system.

Table 1. Chemical composition of iron ore in wt.% according to X-ray fluorescence (XRF) analysis.

Fe (Total)	46.98
SiO ₂	9.58
CaO	4.38
Al ₂ O ₃	5.43
MgO	0.43
MnO	0.23
P ₂ O ₅	2.72
Na ₂ O	0.59
K ₂ O	0.04
S	0.89
Zn	0.08

Mechanochemical reactions between iron ore and carbon dioxide were performed at room temperature and elevated CO₂ pressure (10–30 bar). Planetary ball mill Retsch PM100 was operated at 200 to 400 revolutions per minute. The vessel for the ball milling was a stainless-steel jar of 50 mL volume capable of holding up to 100 bar gas pressure. High purity CO₂ gas (Airgas, 99.999%) was loaded into the reactor at different pressures together with 3.00 g of iron ore and 0.5 mL of water. The average temperature in the reactor during the ball milling process was 32 °C. The mechanochemical reaction was run for different periods, and each 1 h milling interval was followed by half an hour cooling interval to avoid the overheating of the sample. The powder to balls (stainless steel) weight ratio was 2:27. The reactor was flushed several times with CO₂ gas to ensure a pure CO₂ atmosphere inside the reactor. Thermogravimetric analysis (TGA) and differential scanning calorimetry (DSC) were conducted in a temperature range of 25 to 1000 °C using a TA Instruments SDT Q600 instrument. Experiments were performed in air and Ar atmospheres with a heating rate of 10 °C/min. Powder X-ray diffraction patterns were collected using Bruker GADDS/D8 diffractometer equipped with Apex Smart CCD Detector and molybdenum rotating anode. Collected 2D diffraction patterns were integrated using Fit2D software [18]. Quantitative phase analysis of the samples was performed using the Rietveld method and GSAS package [19,20]. The CO₂ sorption capacity was calculated using the results generated by the Rietveld refinement of XRD patterns. Raman spectroscopy characterization was used to identify carbon in siderite decomposition products. A continuous-wave (CW) argon ion (Ar+) laser (model 177G02, Spectra Physics) of 514.4 nm in wavelength was used as a source of monochromatic radiation. Backscattered Raman spectra were collected by a high-throughput holographic imaging spectrograph (model HoloSpec f/1.8i, Kaiser Optical Systems) with volume transmission gratings, a holographic notch filter, and thermoelectrically cooled charge-coupled device (CCD) detector (Andor Technology). The spectra were usually collected with 10 min exposure.

3. Results

3.1. Iron Ore Characterization

The iron ore sample was analyzed by XRD technique. As shown in Figure 1, Fe can be found in the form of hematite Fe₂O₃ (JCPDS card number #00-072-0469), goethite FeOOH (JCPDS card number #00-081-0462), and siderite FeCO₃ (JCPDS card number #00-029-0696).

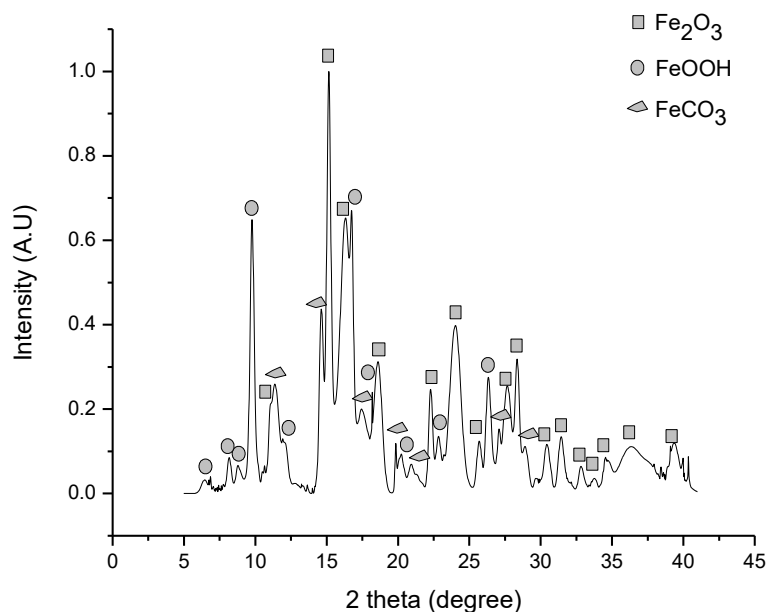


Figure 1. XRD pattern of iron ore sample.

Rietveld refinement shows that iron ore is composed of Fe_2O_3 (48.02%), FeCO_3 (21.15%), and FeOOH (30.83%). These results defined chemical reactions (1) and (2).

Reactions (1) and (2) use Fe iron as a reducing agent. Moreover, Sulfur (S) included in the iron ore in the form of sulfate or sulfide can act as a reducing agent. In García et al. [21], siderite is obtained from hematite, carbon dioxide, sulfur dioxide, and water at suitable conditions.

The regeneration reaction studied in this work is shown below:



After regeneration, products can be further recycled back and used in a new carbonation reaction to complete the cycle.

3.2. Thermodynamics Simulation of Iron Ore Carbonation

FACTSAGE software and the databases therein, FACT-F*A*C*T 5.0, SGPS-SGTE, and SGSL were used to verify the thermodynamic feasibility of the carbonation process at equilibrium for the system iron ore– CO_2 . According to XRD analysis and chemical composition of the ore, carbonation simulations were performed considering iron ore as a mixture of hematite and goethite. Carbonation in ball milling was simulated at a temperature of 32 °C (the average temperature measured in the reactor) and CO_2 pressures between 1 and 50 bar. As can be seen in Figure 2, siderite is stable at those conditions.

Figure 3 shows simulations at HTHP conditions for iron ore carbonation in the temperature range of 25 to 325 °C and CO_2 pressures of 10 and 50 bar. Figure 3a,b do not include Fe in the reaction, while Figure 3c,d include this metallic element. The presence of siderite is evident in all cases. The stability of siderite increased with pressure. This behavior was observed in both systems. It is clear that when Fe is included in the system, the decomposition temperature of siderite increased for the same CO_2 pressure. For example, the siderite decomposition temperature at 50 bar began at 150 and 225 °C for systems without and with Fe, respectively, revealing the advantage of including Fe due to higher temperatures favoring the thermodynamic conditions for carbonation.

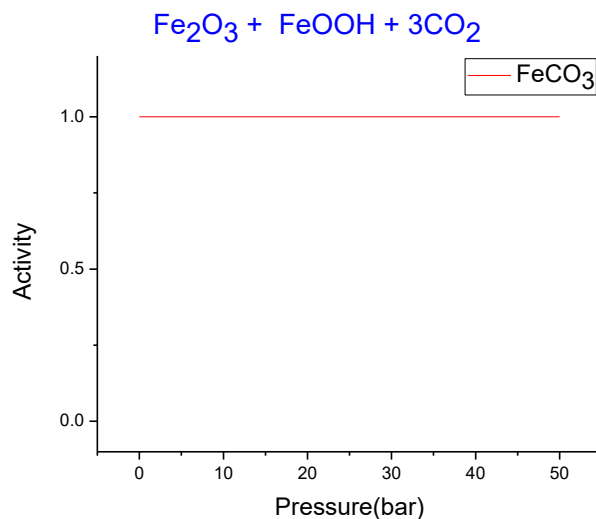


Figure 2. FACTSAGE simulation of siderite stability at 32 °C and various pressures for the system, iron ore–CO₂.

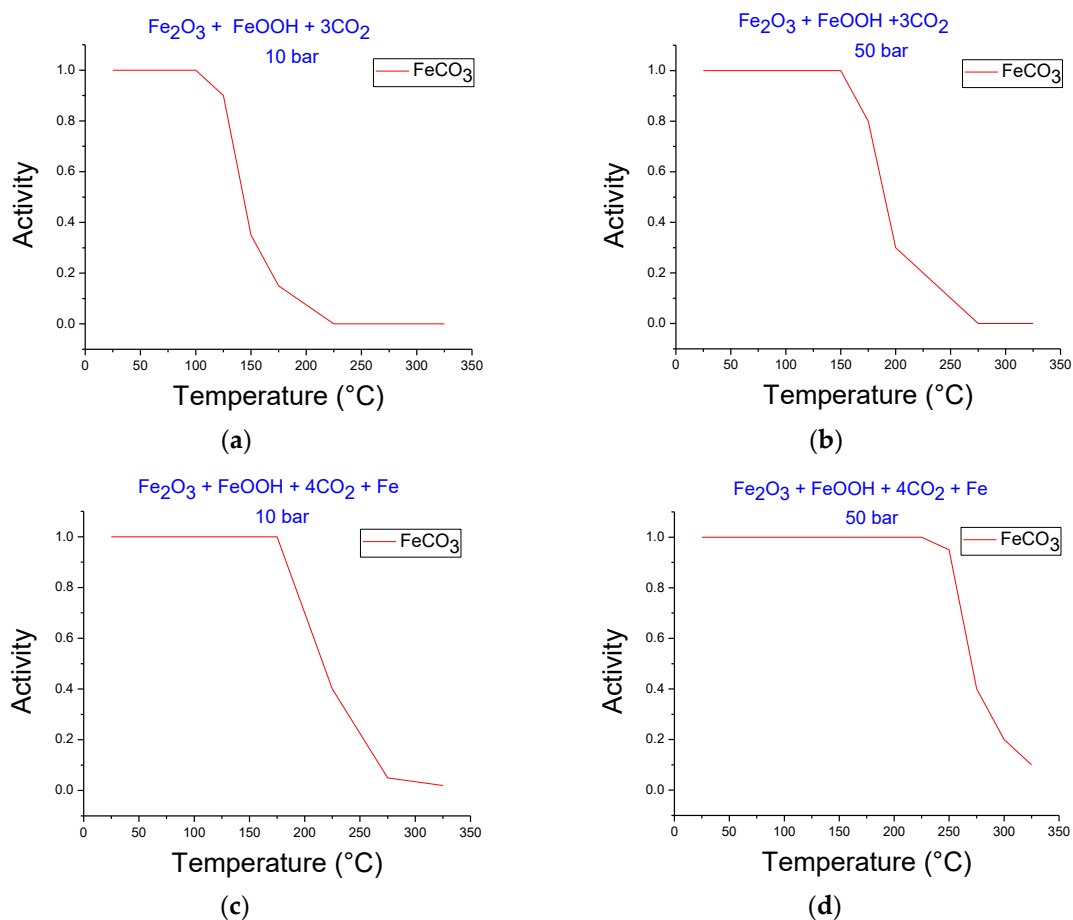


Figure 3. FACTSAGE simulations at various temperatures for the system iron ore–CO₂, (a) 10 bar, (b) 50 bar, and for the system iron ore–CO₂–Fe (c) 10 bar, (d) 50 bar.

3.3. Iron Ore Carbonation in Mechanochemical Process

Siderite yield in the carbonation reaction increased (JCPDS card number # 029-0696) as a result of carbonation by the ball milling method. Figure 4 shows the increases in iron carbonate formation at 30 bar, 400 rpm, 32 °C, and 20 h of time reaction.

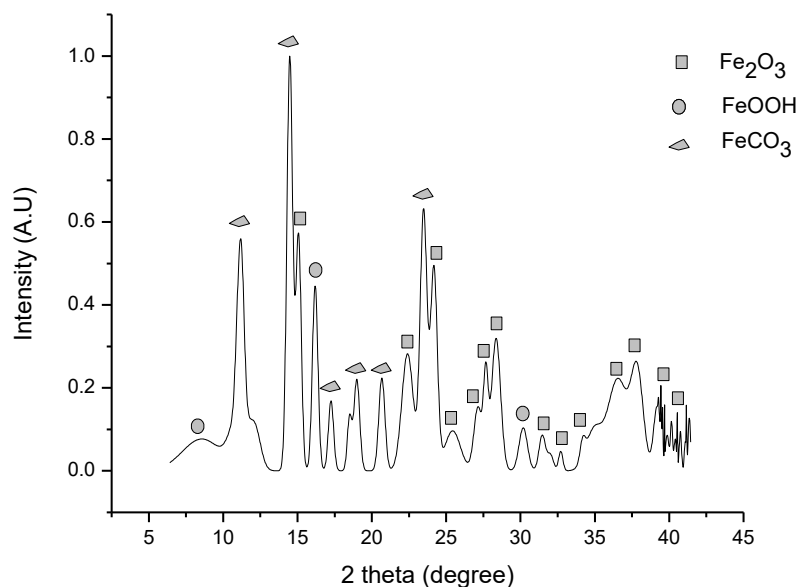


Figure 4. Carbonation of iron ore in ball milling at 30 bar, 400 rpm, 32 °C, and 20 h of reaction time.

Initially, the experiments were performed without water, but the siderite amount did not change. That can be related to kinetics limitations. It is clear that water acts as a catalyst in the carbonation process of metal oxides [13,22]. Figure 4 reveals that a considerable amount of siderite can be obtained by 20 h of milling. For those conditions, the CO₂ capture capacity of hematite and goethite is 0.1643 g CO₂/g sorbent or 3.7341 mmol CO₂/g sorbent calculated from the Rietveld refinement of the XRD pattern. This value translates to a 26.82% conversion rate. The calculation was performed, taking into account the initial amount of FeCO₃ contained in the ore and that the amount of initial absorbent is the sum of the weights of goethite and hematite.

Table 2 shows the calculations of CO₂ capture capacity at different conditions of pressure, revolution speed, and duration of the reaction. As can be seen in the table, the CO₂ capture at the same temperature by iron ore increased at higher pressures and longer reaction times.

Table 2. CO₂ capture capacity of iron ore at different conditions of pressure, revolution speed, and time reaction in the mechanochemical process.

Pressure (bar)	Revolution Speed (rev/min)	Time Reaction (h)	CO ₂ Capture Capacity (mmol CO ₂ /g sorbent)
10	400	3	1.075
10	400	6	1.9523
20	400	3	1.7545
20	400	6	2.9204
20	200	3	0.4318
30	200	3	0.6864
30	200	6	0.8545

Additionally, values in Table 2 reveal that the ball milling process is affected by the revolution speed of the ball mill. At faster speeds, the siderite yield increased due to the transfer of higher kinetic energy, promoting the appearance of defects, which generate more active sites in goethite and hematite, facilitating the reaction with CO₂. According to [23] in the ball milling process, there is a critical revolution speed above which the balls will be pinned to the inner walls of the vial and do not fall to exert any impact force. In these experiments, the speeds of revolution were kept below the critical speed.

3.4. Iron Ore Carbonation in the HTHP Process

Using this method, neither using graphite as a reducing agent and water as a catalyst nor iron as a reducing agent and no water, the siderite yield was increased. Figure 5 confirms an increase of siderite yield (JCPDS card number #00-029-0696) as a result of carbonation by the HTHP method at 50 bar, 100 °C, and 4 h with the addition of metallic iron and water to iron ore. For these conditions, the CO₂ capture capacity was 0.2393 g CO₂/g sorbent or 5.4392 mmol CO₂/g sorbent calculated from the Rietveld refinement of the XRD pattern. This value translates to a 39.08% conversion rate.

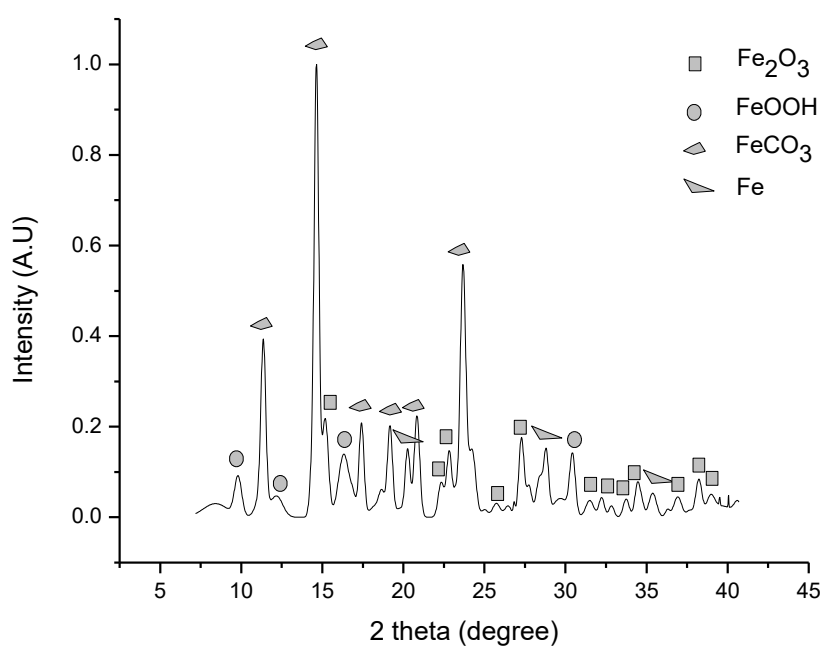


Figure 5. Carbonation of iron ore in the thermo pressure process at 50 bar, 100 °C, and 4 h of time reaction.

Table 3 presents the CO₂ capture capacity at different conditions of pressure, temperature, and reaction time. Longer reaction times increased the CO₂ capture for all cases. Siderite stability at higher temperatures decreased. For example, at 200 °C, 50 bar, and 4 h, a decrease of 53.2% in siderite formation was evidenced compared to 150 °C. These considerations can be confirmed with FACTSAGE simulations, which showed that at 50 bar, siderite began to decompose at temperatures around 200 °C. In this case, it can be supposed that the decomposition temperature is lower due to the presence of water. The CO₂ capture capacity of iron ore increased at higher pressures while keeping the temperature and reaction time constant, confirming the same effect observed in the mechanochemical process.

Table 3. CO₂ capture capacity of iron ore at different conditions of pressure, temperature, and reaction time in the high temperature–high pressure (HTHP) process.

Pressure (bar)	Temperature (°C)	Reaction Time (h)	CO ₂ Capture Capacity (mmol CO ₂ /g Sorbent)
30	100	4	4.7927
30	200	1	1.6629
30	200	4	1.9945
50	100	1	2.9118
50	100	4	5.4392
50	150	4	5.7069
50	200	4	2.6713

3.5. Thermal Decomposition of Siderite Studied by Thermogravimetric Analysis

The siderite decomposition reaction was studied on two samples. The first one was obtained by the mechanochemical process at 30 bar of CO₂ pressure, 400 rpm, and 20 h of reaction time, and the second one was obtained at 50 bar of CO₂ pressure, 100 °C, and 4 h of reaction time by the HTHP process. The decomposition temperature of siderite was experimentally identified using thermogravimetric analysis. Figure 6a,b show the TG–DSC plots for siderite obtained in mechanochemical and HTHP processes, respectively, in an argon atmosphere.

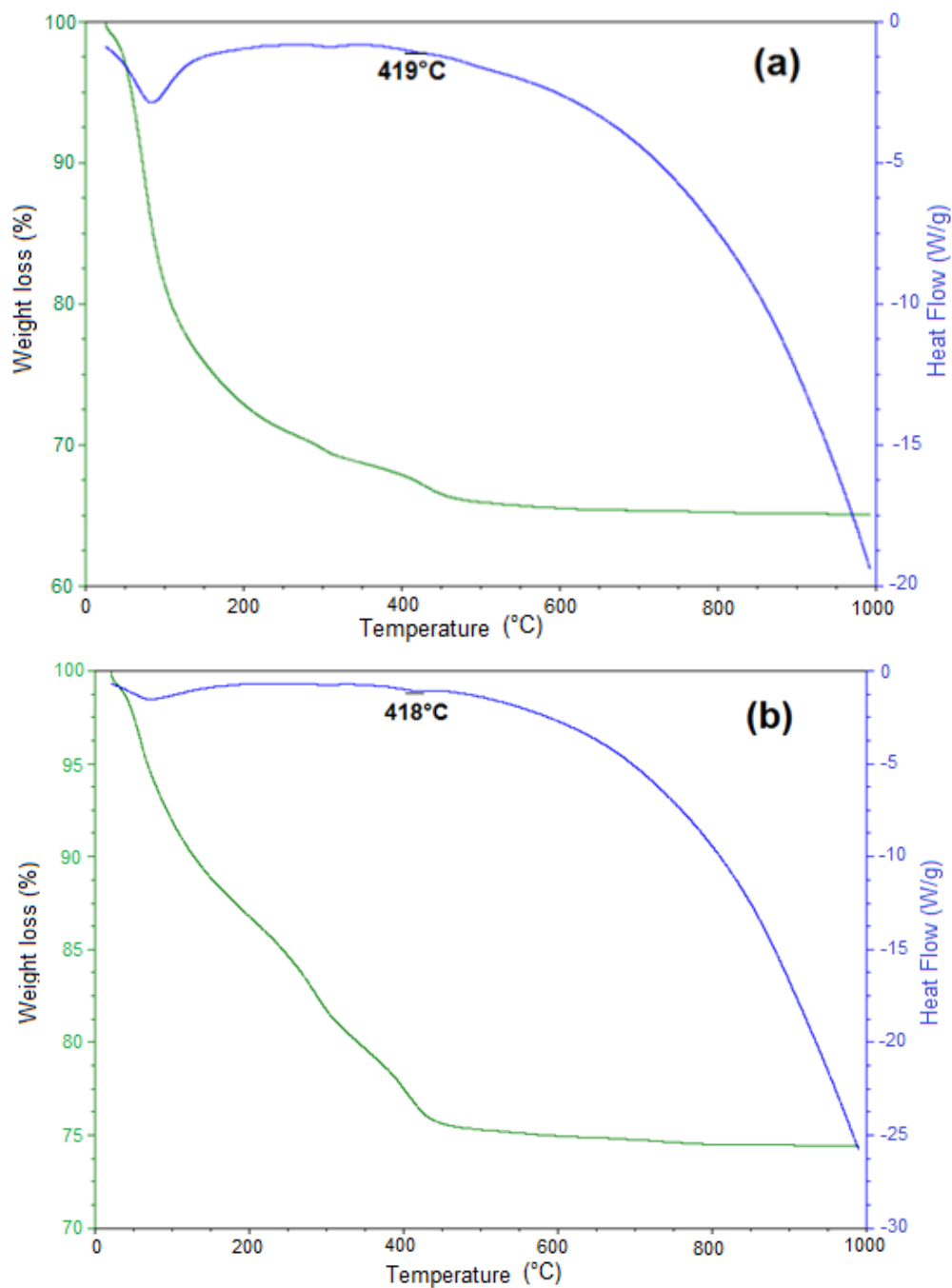


Figure 6. Thermogravimetric (TG)-heat flow plot of thermal decomposition of the product formed at 30 bar CO₂ pressure, 400 rpm, and 20 h (a), and at 50 bar, 100 °C, 4 h (b), heating rate 10 °C/min in an argon atmosphere.

The reaction mechanism for decomposition of siderite samples synthesized from pure iron oxides without water in an argon atmosphere was studied in [14]. Here, according to the thermal gravimetry (TG) plots, mass losses around 100 °C occurred for both plots. They were equivalent to 18 wt% and 6 wt%, respectively, and corresponded to the release of adsorbed water by iron ore. The release of CO₂ started from 100 °C. Some research works have reported that in the temperature interval between 250 and 375 °C, there are losses of weight corresponding to the dehydration of the goethite phase and iron hydroxides [24,25].

The thermal decomposition of siderite was significant at the temperature range of 100 to 420 °C. According to [14], this range reaches higher temperatures compared to the decomposition temperature of siderite synthesized from pure iron oxides, due to siderite decomposition temperature increasing with decreasing purity [15,26]. Patterson et al. [27] found that magnesium, manganese, or calcium increases the siderite decomposition temperature.

To identify the products after calcination, the siderite sample obtained by the mechanochemical reaction at 30 bar of CO₂ pressure, 400 rpm, and 20 h of reaction time was decomposed. The X-ray diffraction pattern in Figure 7 evidences the presence of magnetite (JCPDS # 001-1111), hematite (JCPDS # 00-001-1053), and graphite (JCPDS # 00-026-1079) after decomposition in a vacuum at 300 °C for 1 h. As can be seen, at this temperature, siderite was completely decomposed. The same products were identified for decomposed siderite, obtained by the HTHP process, and under the same decomposition conditions.

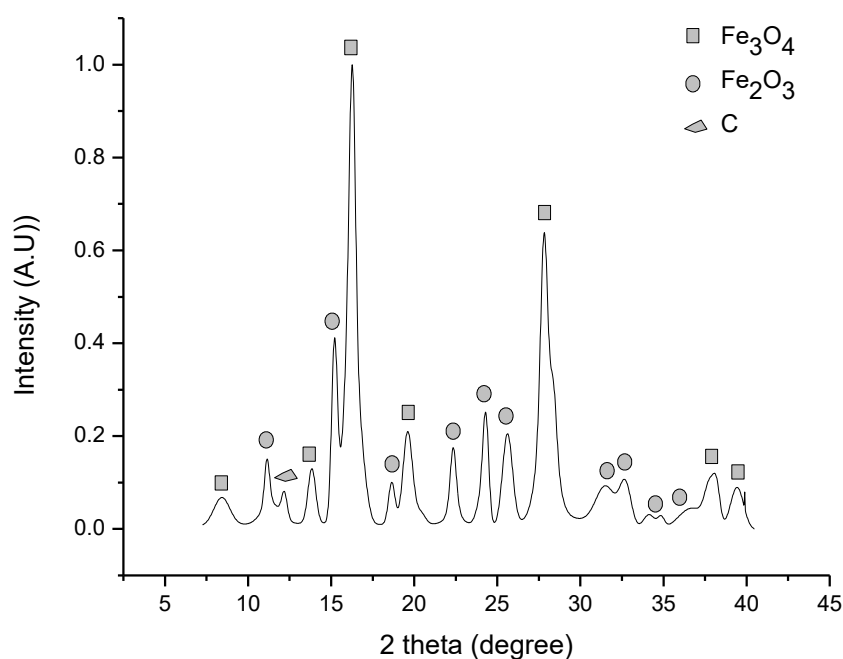


Figure 7. XRD pattern after siderite decomposition at 300 °C in a vacuum. Magnetite, hematite, and graphite were identified.

Raman spectroscopy is a suitable technique for graphite identification, due to its high sensitivity to highly symmetric covalent bonds with little or no natural dipole moment. The carbon–carbon bonds that make up these materials fit this criterion perfectly, and as a result, Raman spectroscopy is highly sensitive to these materials and able to provide a wealth of information about their structure. Every band in the Raman spectrum corresponds directly to a specific vibrational frequency of a bond within the molecule. The 1582 cm⁻¹ band of graphite is known as the G band, and at 1370 cm⁻¹, a characteristic line appears, which is named D mode for a disorder-induced mode of graphite [28–30].

According to Figure 8, decomposed siderite at 300 °C in vacuum evidences the presence of graphite, by mean of peaks at 1582 cm⁻¹ and 1370 cm⁻¹. Figure 8a,b show the Raman patterns of decomposed siderite produced by mechanochemical and HTHP processes, respectively. These results confirm that reaction (3) occurs during siderite decomposition obtained by both ball milling and HTHP.

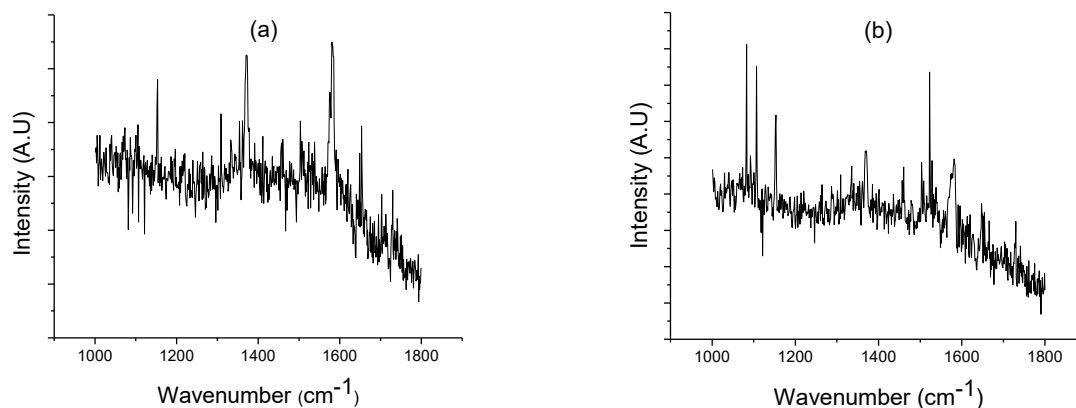


Figure 8. Raman pattern of decomposed siderite from processes, (a) mechanochemical (b), HTHP.

3.6. Carbonation–Calcination Cycles

Samples of decomposed siderite were studied in various cycles in CO₂ absorption/release reactions to confirm if the materials can be reused. Initially, using the two calcinated samples, there was no CO₂ capture, neither in mechanochemical nor in HTHP

For the mechanochemical method at 30 bar CO₂ pressure, 400 rpm, 20 h, adding water to the samples, siderite yield was accomplished. After recarbonation, samples were decomposed at 300 °C in a vacuum. Table 4 shows the CO₂ capture capacity of the transformed material for several cycles in the mechanochemical process.

Table 4. CO₂ capture capacity for several cycles of carbonation–calcination using the mechanochemical process.

N° Cycle, Carb-Calc	Added Extra Substances	CO ₂ Capture Capacity (mmol CO ₂ /g Sorbent)
1	Water	3.7341
2	Water	4.1354
3	Water	6.2158
4	Water	6.9611

The addition of magnetite as a new chemical to the absorbent mixture and carbon as a new reducing agent improved the CO₂ capture capacity in subsequent cycles. Here, one additional carbonation reaction is:



Hence, iron ore can be used for multiple cycles according to the combination of (1), (2), (3), and (4) reactions.

For HTHP, the recarbonation was studied at 50 bar, 100 °C, and 4 h. Graphite was used as a reducing agent in the first place due to its availability and cost. There was no siderite formation after adding extra-graphite to the mixture. It was necessary to add iron and water to achieve new carbonation. The iron addition is not propitious in terms of cost. After recarbonation, samples were decomposed at 300 °C in a vacuum. Table 5 shows the CO₂ capture capacity of material in the second and third cycles. As can be seen, it was necessary to include extra iron in both cycles. Here, only three cycles were studied because CO₂ capture capacity decreases dramatically during cycles.

Table 5. CO₂ capture capacity for several cycles of carbonation–calcination using the HTHP process.

N° Cycle, Carb-Calc	Added Extra Reactants	CO ₂ Capture Capacity (mmol CO ₂ /g Sorbent)
1	Water, iron	5.4392
2	Water, iron	4.8687
3	Water, iron	2.7125

3.7. Discussion

It is clear that the addition of water to the mixtures facilitates CO₂ sorption and thus, affects the reactivity and capacity of the materials. The presence of moisture increases the mobility of alkaline ions and thus, accelerates the reactions [13,31–33]. Here, in the two methods of carbonation studied, reactions without water did not allow the siderite formation due to kinetics limitations. According to [13], water on the sorbent surface before and after calcinations facilitates the reaction with CO₂, which results in the formation of CO₃²⁻ and H⁺ ions. Free Fe⁺² ions can further react with CO₃²⁻ to form FeCO₃. The presence of water has a dual effect. It not only helps CO₂ uptake of sorbent but also affects the siderite stability [13,14].

With increasing siderite formation over time, its layer thickens, which inhibits the contact between Fe⁺² and CO₃²⁻ harming the formation of new siderite. The mechanochemical process provides a way to remove the outer layer of FeCO₃; this layer is generally nonporous. This fluidization regime allows the carbonation reaction to remain more active [14,34,35]. This is likely the reason the carbonation process did not need an extra-reducing agent, such as iron, to obtain siderite in all of the cycles, which is an advantage compared with the HTHP process, which needed metallic iron. Initially, the presence of iron allowed high levels of CO₂ capture; however, with cycles, the actives sites vanished, and the CO₂ capture was practically negligible.

The advantage of the fluidization regime used in the mechanochemical process can be explained through kinetics. Figure 9 shows the siderite yield vs. time for two samples at 20 bar CO₂ pressure and 32 °C. The first one was treated at 400 rpm and the other one at 200 rpm. As was explained above, the carbonation depends strongly on the revolution speed for the same conditions of pressure and temperature, if the revolution speed is lower than the critical speed. The product yield at 3 h of reaction time and 400 rpm is about three times higher than the mass gained at 200 rpm speed.

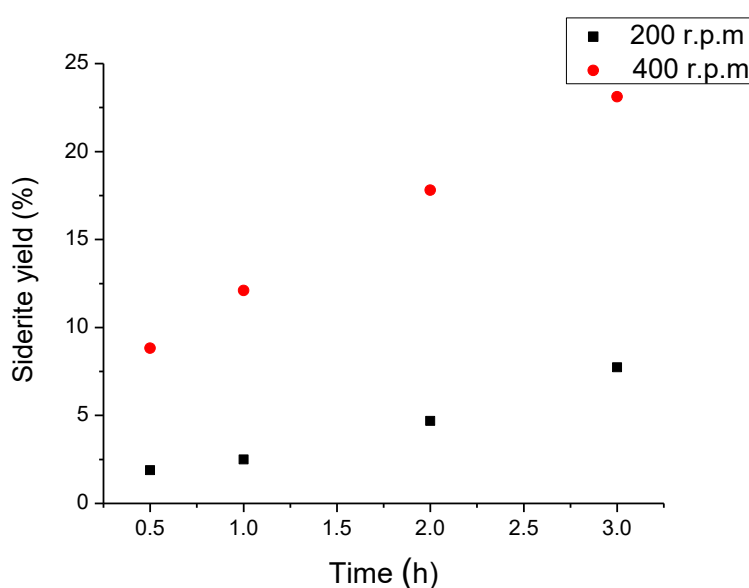


Figure 9. Siderite formation as a function of rotation speed at 20 bar CO₂ pressure and 32 °C in the ball milling process.

According to Alkaç and Atalay [36], using the mass fractional conversion x with respect to time, it is possible to calculate $f(x)$, the reaction model, which comprises the particular fractional conversion and related mechanism in terms of mathematical equations [15,36]. If $f(x)$ vs. t has high linearity, it indicates a suitable fitting for a given model and the slope gives the value of the rate constant, k , at a fixed temperature. Constant k is directly proportional to the reaction rate. For example, Figure 10 depicts $f(x)$ as a function of time, taking the Jander three dimensional diffusion model which presented high linearity. This model expresses $f(x)$ as

$$f(x) = [1 - (1 - x)^{\frac{1}{3}}]^2 \quad (5)$$

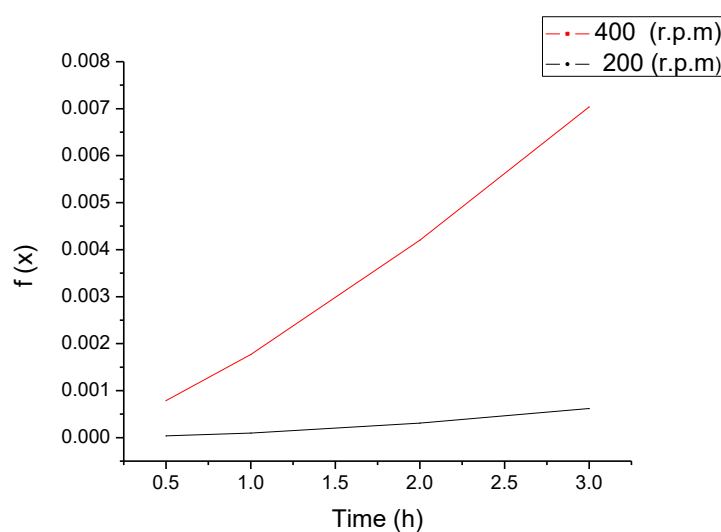


Figure 10. The Jander three-dimensional diffusion model evaluated for fractional mass conversion values (x) as a function of time at 20 bar and 32 °C in the ball milling process.

The slopes represent k according to the expression above. Hence, if the machine operates to 400 rpm, the rate constant increases 4.14 times compared to k at 200 rpm. Hence, if the kinetics energy transferred to the absorbent is bigger, carbonation conditions improve [37,38].

Another important consequence of the mechanochemical treatment is the improvement in calcination conditions. Some researches [39,40] have reported siderite, which has been treated in the ball milling process, as having lower decomposition temperatures.

According to carbonation reactions, it is possible to establish a projection of the amount of raw material that would be used in large-scale CO₂ emissions. Table 6 shows the needed material amount to capture 1 ton of CO₂ in carbonation reactions, assuming 100% conversion. The amount of formed siderite is 2.63 tons in both reactions.

Table 6. Amount of raw material needed to capture 1 ton of CO₂ in several carbonation reactions, assuming 100% of conversion yield.

Reaction	Material	Amount (ton)
$\text{Fe}_2\text{O}_3(\text{s}) + \text{Fe} + 3\text{CO}_2(\text{g}) \rightarrow 3\text{FeCO}_3(\text{s}) + \text{H}_2\text{O}$	Fe ₂ O ₃	1.21
	Fe	0.42
$2\text{FeOOH}(\text{s}) + \text{Fe} + 3\text{CO}_2(\text{g}) \rightarrow 3\text{FeCO}_3(\text{s}) + \text{H}_2\text{O}$	FeOOH	1.35
	Fe	0.42

In terms of steel production in a blast furnace, to produce one ton of steel, around 1.8 tons of CO₂ emissions are generated. Here, for carbonation by mechanochemical interaction, 3.43 tons

of iron ore are needed operating at 30 bar, 400 rpm for 36 h for the almost total transformation of iron ore. Otherwise, using HTHP, 2.26 tons of iron ore and 0.75 tons of metallic iron are needed as initial materials. However, the capture is reduced to a maximum of 43.15% in HTHP due to kinetics limitations and surface area conditions. Since carbonation by the mechanochemical method has remarkable advantages, the amount of the recovered material is calculated from the calcination reaction (3). In this case, 4.37 tons of siderite will be transformed into 2.91 tons of magnetite, 0.073 tons of carbon, and 1.38 tons of CO₂. Magnetite and carbon will be used in the next cycle as sorbent and reducing agent, respectively, and pure CO₂ can be used in industrial applications.

Another important point to consider is the energy needed in each process. According to [41], the total spent energy in ball milling can be calculated as a function of the filling factor of the reactor, ball mass, ball diameter, number of balls, reaction time, rotation speeds of plate and reactor, the radius of plate and reactor, and sample mass. A sample processed at 30 bar, 400 rpm, and 3 h consumes 14.062 W-h per gram of absorbent having a CO₂ capture capacity of 2.7816 mmol CO₂/g sorbent. In HTHP, the energy can be calculated by multiplying the values of electrical current, electrical voltage, a factor of heat losses, and time reaction. The power factor was taken as one, due to the total impedance in the electrical circuit that warms the reactor being completely resistive. To compare the expenses of energy demands from the mechanochemical and HTHP processes, similar values of CO₂ capture capacities were taken. Hence, the spent energy to process a sample at 50 bar, 100 °C, and 1 h, which produced a CO₂ capture capacity of 2.9118 mmol CO₂/g sorbent was calculated. This process needed 41.58 W-h per gram. This energy is almost three times larger than the energy in the mechanochemical method. In addition, the CO₂ pressure is higher which is an extra penalty.

4. Conclusions

Iron ore was studied for CO₂ capture. The CO₂ capture capacity was evaluated for two methods, ball milling and HTHP. Water was always added to accomplish carbonation. Higher levels of capture were achieved at higher pressures and reaction times. Faster revolution speed allowed an increase in the siderite formation in ball milling. In HTHP, carbonation reactions were favored by temperatures between 100 and 150 °C, but at 200 °C, an inverse reaction was observed. The range of regeneration of iron oxides was identified between 100 °C and 420 °C in both methods, reaching higher temperatures than the siderite decomposition temperatures formed from synthetic iron oxides, due to decomposition temperature increases with decreasing purity. Magnetite and carbon were identified as decomposition products. It was necessary to add water to accomplish re-carbonation in the mechanochemical process while in the HTHP process, metallic iron and water were needed. Carbonation by the mechanochemical process was studied for four carbonation–calcination cycles presenting suitable conditions, while HTHP was only studied for three cycles due to its CO₂ capture capacity decreasing. The amounts of hematite, goethite, and metallic iron needed to capture 1 ton of CO₂ in carbonation reactions were calculated. A projection of the material needed to carbonate, as well as the material recovered in the calcination, for a real application was carried out. Kinetics and energy requirements confirmed the advantages of carbonation by mean of the mechanochemical process compared to the HTHP method.

Author Contributions: All authors contributed to the manuscript. E.Y.M.M. and V.D. proposed the initial idea; A.D. designed and managed the technological equipment; E.Y.M.M. and V.D. performed the simulations; A.D., E.Y.M.M. and V.D. performed the experimentation. V.D. and E.Y.M.M. wrote the manuscript; J.C., A.S.S., E.V.L. and S.K.S. improved the manuscript.

Funding: This research received no external funding.

Acknowledgments: The authors acknowledge the financial support by Departamento Administrativo de Ciencia, Tecnología e Innovación, Colciencias in Colombia. The work in part is supported by the NSF Geophysics Program (EAR 1723185).

Conflicts of Interest: The authors declare no conflict of interests.

References

1. Sanz-Pérez, E.; Murdock, C.; Didas, S.; Jones, C. Direct Capture of CO₂ from Ambient Air. *Chem. Rev.* **2016**, *116*, 11840–11876. [[CrossRef](#)] [[PubMed](#)]
2. Wiers, B. Capture of Carbon Dioxide from Air and Flue Gas in the Alkylamine-Appended Metal–Organic Framework mmen-Mg₂(dobpdc). *J. Am. Chem. Soc.* **2012**, *7056*–7065. [[CrossRef](#)]
3. Yu, C.H.; Huang, C.H.; Tan, C.S. A Review of CO₂ capture by absorption and adsorption. *Aerosol Air Qual. Res.* **2012**, *12*, 745–769. [[CrossRef](#)]
4. Kim, Y.; Worrell, E. International comparison of CO₂ emission trends in the iron and steel industry. *Energy Policy* **2002**, *30*, 827–838. [[CrossRef](#)]
5. Kumar, S.; Saxena, S. A comparative study of CO₂ sorption properties for different oxides. *Mater. Renew. Sustain. Energy* **2014**, *1*, 2. [[CrossRef](#)]
6. Han, K.; Ahn, C.; Lee, M.S. Performance of an ammonia-based CO₂ capture pilot facility in iron and steel industry. *Int. J. Greenh. Gas Control* **2014**, *27*, 239–246. [[CrossRef](#)]
7. Pannocchia, G.; Puccini, M.; Seggiani, M.; Vitolo, S. Experimental and modeling studies on high-temperature capture of CO₂ Using Lithium Zirconate Based Sorbents. *Ind. Eng. Chem. Res.* **2007**, *46*, 6696–6706. [[CrossRef](#)]
8. Kumar, A.; Ramaprabhu, S. Nano magnetite decorated multiwalled carbon nanotubes: A robust nanomaterial for enhanced carbon dioxide adsorption. *Energy Environ. Sci.* **2011**, *4*, 889–895.
9. Ho, M.; Leamon, M.; Allinson, D.; Wiley, D. Economics of CO₂ and mixed gas geosequestration of flue gas using gas separation membranes. *J. Membr. Sci.* **2006**, *45*, 2546–2552.
10. Zhao, L.; Rienache, E.; Menzer, R.; Blum, L.; Stolen, D. A parametric study of CO₂/N₂ gas separation membrane processes for post-combustion capture. *J. Membr. Sci.* **2008**, *325*, 284–294. [[CrossRef](#)]
11. Zaman, M.; Hyung Lee, J. Carbon capture from stationary power generation sources: A review of the current status of the technologies. *Korean J. Chem. Eng.* **2013**, *30*, 1497–1526. [[CrossRef](#)]
12. Salvador, C.; Lu, D.; Anthony, E.; Abanades, J. Enhancement of CaO for CO₂ capture in an FBC environment. *Chem. Eng.* **2003**, *96*, 187–195. [[CrossRef](#)]
13. Kumar, S.; Drozd, V.; Durygin, A.; Saxena, S. Capturing CO₂ Emissions in the iron industries using a magnetite–iron mixture. *Energy Technol.* **2016**, 1–5. [[CrossRef](#)]
14. Mora, E.; Sarmiento, A.; Lopez, E.; Drozd, V.; Durigyn, A.; Saxena, S.; Chen, J. Iron oxides as efficient sorbents for CO₂ capture. *J. Mater. Res. Technol.* **2019**, *8*, 2944–2956. [[CrossRef](#)]
15. Gotor, F.; Macias, M.; Ortega, A.; Criado, J. Comparative study of the kinetics of the thermal decomposition of synthetic and natural siderite samples. *Phys. Chem. Miner.* **2000**, *27*, 475–503. [[CrossRef](#)]
16. Dhupe, A.; Gokarn, N. Studies in the Thermal Decomposition of Natural Siderites in the esence of Air. *Int. J. Miner. Process.* **1990**, *28*, 209–220. [[CrossRef](#)]
17. Fosbol, P.; Thompsen, K.; Stenby, E. Review and recommended thermodynamic properties of FeCO₃. *Corros. Eng. Sci. Technol.* **2013**, *45*, 115–135. [[CrossRef](#)]
18. Hammersley, A. *ESRF Internal Report, ESRF97HA02T, FIT2D: An Introduction and Overview*; European Synchrotron Radiation Facility: Grenoble, France, 1997.
19. Toby, B. EXPGUI, a graphical interface for GSAS. *J. Appl. Cryst.* **2001**, *34*, 210–221. [[CrossRef](#)]
20. Larson, A.; Von Dreele, R. *General Structure Analysis System (GSAS)*; Report LAUR 86-748; Los Alamos National Laboratory: Los Alamos, NM, USA, 2004.
21. Garcia, S.; Rosenbauer, R.; Palandri, J.; Maroto-Valer, M. Sequestration of non-pure carbon dioxide streams in iron oxyhydroxide-containing saline repositories. *Int. J. Greenh. Gas Control* **2012**, *7*, 89–97. [[CrossRef](#)]
22. Kumar, S.; Saxena, S.; Drozd, V.; Durygin, A. An experimental investigation of mesoporous MgO as a potential pre-combustion CO₂ sorbent. *Mater. Renew. Sustain. Energy* **2015**, *4*. [[CrossRef](#)]
23. Suryanarayana, C. Mechanical alloying and milling. *Prog. Mater. Sci.* **2001**, *46*, 1–184. [[CrossRef](#)]
24. Liu, C.; Shih, S. Kinetics of the reaction of iron blast furnace slag/hydrated lime sorbents with SO₂ at low temperatures: Effects of the presence of CO₂, O₂, and NO_x. *Ind. Eng. Chem.* **2009**, *48*, 8335–8340. [[CrossRef](#)]
25. Betancur, J.; Barrero, D.; Greneche, F.; Goya, F. El efecto del contenido de agua en la magnetita y en las propiedades estructurales de la goethita. *J. Alloy. Comp.* **2004**, *369*, 247–251. [[CrossRef](#)]
26. Gallagher, P.; Warne, S. Thermogravimetry and thermal decomposition of siderite. *Thermochim. Acta* **1980**, *43*, 253–267. [[CrossRef](#)]

27. Patterson, J.; Levi, J. Relevance of carbonate minerals in the processing of Australian oil shales. *Fuel* **1991**, *70*, 1252–1259. [[CrossRef](#)]
28. Hodkiewicks, J. *Characterizing Carbon Materials with Raman Spectroscopy*; Thermo Fisher Scientific: Madison, WI, USA, 2010.
29. Reitch, S.; Thomsen, C. Raman spectroscopy of graphite. *R. Soc.* **2004**, *362*, 2271–2278. [[CrossRef](#)]
30. Wang, Y.; Alsmeyer, S.; McCreery, S. Raman Spectroscopy of Carbon Materials: Structural Basis of Observed Spectra. *Chem. Mater.* **1990**, *2*, 557–563. [[CrossRef](#)]
31. Kummar, S. The effect of elevated pressure, temperature and particles morphology on the carbon dioxide capture using zinc oxide. *J. CO₂ Util.* **2014**, *8*, 60–66. [[CrossRef](#)]
32. Hassanzadeh, A.; Abbasian, J. Regenerable MgO-based sorbents for high-temperature CO₂ removal from syngas: 1. Sorbent development, evaluation, and reaction modeling. *Fuel* **2010**, *89*, 1287–1297. [[CrossRef](#)]
33. Sun, J.; Yang, Y.; Guo, Y.; Xu, Y.; Li, W.; Zhao, A.; Liu, W.; Lu, P. Stabilized CO₂ capture performance of wet mechanically activated dolomite. *Fuel* **2018**, *222*, 334–342. [[CrossRef](#)]
34. Ounoughene, G.; Buskens, E.; Santos, R.; Cizer, O.; Van Gerven, T. Solvochemical carbonation of lime using ethanol: Mechanism and enhancement for direct atmospheric CO₂ capture. *J. CO₂ Util.* **2018**, *26*, 143–151. [[CrossRef](#)]
35. Benitez, M.; Valverde, J.; Perejon, A.; Sanchez, P.; Perez, L. Effect of milling mechanism on the CO₂ capture performance of limestone in the Calcium Looping process. *Chem. Eng. J.* **2018**, *346*, 549–556. [[CrossRef](#)]
36. Alkaç, D.; Atalay, U. Kinetics of thermal decomposition of Hekimhan–Deveci siderite ore samples. *Int. J. Miner. Process.* **2008**, *87*, 120–128. [[CrossRef](#)]
37. Rigopoulos, I.; Vasiliades, M.; Ioannou, I.; Esftathiou, A.; Godelistsas, A.; Kyratsy, T. Enhancing the rate of ex situ mineral carbonation in dunites via ball milling. *Adv. Powder Technol.* **2016**, *27*, 360–371. [[CrossRef](#)]
38. Rigopoulos, I.; Delimitis, A.; Ioannou, I.; Esftathiou, A.; Kyratsy, T. Effect of ball milling on the carbon sequestration efficiency of serpentinized peridotites. *Miner. Eng.* **2018**, *120*, 66–74. [[CrossRef](#)]
39. Criado, J.; Gonzalez, M.; Macias, M. Influence of grinding on both the stability and thermal decomposition mechanical of siderite. *Thermochim. Acta* **1988**, *135*, 219–223. [[CrossRef](#)]
40. Bradley, W.; Burst, J.; Graf, D. Crystal chemistry and differential thermal effect of dolomite. *Am. Mineral.* **1953**, *38*, 207–211.
41. Burgio, N.; Lasonna, A.; Magini, M.; Martelli, S.; Padella, F. Mechanical Alloying of the Fe-Zr System. Correlation between Input Energy and End Products. *Il Nuovo Cim. D* **1991**, *13*, 459–476. [[CrossRef](#)]



© 2019 by the authors. Licensee MDPI, Basel, Switzerland. This article is an open access article distributed under the terms and conditions of the Creative Commons Attribution (CC BY) license (<http://creativecommons.org/licenses/by/4.0/>).